Mechanisms of in Situ Scanning Tunnelling Microscopy of Organized Redox Molecular Assemblies

Alexander M. Kuznetsov

The A. N. Frumkin Institute of Electrochemistry of the Russian Academy of Sciences, Leninskij Prospect 31, Moscow 117071, Russia

Jens Ulstrup*

Department of Chemistry, Technical University of Denmark, DK-2800 Lyngby, Denmark

Received: October 12, 1999; In Final Form: September 20, 2000

A theoretical frame for in situ electrochemical scanning tunneling microscopy (STM) of large adsorbed redox molecules is provided. The in situ STM process is viewed as two consecutive interfacial single-step electron transfer (ET) processes with full vibrational relaxation between the steps. The process is therefore a cycle of consecutive molecular reduction and reoxidation. This extends previous approaches where resonance tunneling, or coherent single-channel ET, were in focus. The dependence of the tunneling current on the bias voltage and overvoltage is calculated when both transitions are either fully adiabatic or fully diabatic, and when one transition is fully adiabatic and the other one fully diabatic. A particular feature of the fully adiabatic limit is that each oxidation−reduction cycle is composed of manifolds of individual interfacial ET events at both electrodes, enhancing electron tunneling significantly compared to single-ET. The voltage dependences show spectrocopy-like features. Particularly, the overvoltage dependence has a maximum at the equilibrium potential when the potential distribution in the tunnel gap is symmetric. This is different from resonance and coherent tunneling where the maximum is shifted approximately by the nuclear reorganization Gibbs free energy. Recent data for in situ STM of iron protoporphyrin IX on highly oriented pyrolytic graphite (Tao, N. J. *Phys. Rev. Lett.* **1996**, *76*, 4066−4069) show such a maximum and therefore accord well with sequential two-channel ET. This shows that multiphonon ET theory extended to in situ STM of redox molecules offers a comprehensive frame where distinction between different tunneling mechanisms is feasible.

1. Introduction

The understanding of electron transfer (ET) reactions involving synthetic donor−acceptor complexes or metalloproteins has been brought to a level where most controlling factors have been probed,[1−11] particularly reorganization and driving force, intermolecular recognition, and directional and fluctuational long-range tunnel effects. ET theory is also becoming a guide to the understanding of new *supramolecular* micro- and mesoscopic ET systems,[12,13] holding perspectives for the development of nanoscale devices with appellations such as molecular wires, self-assembled monolayers, electronic rectifiers, and optical reading and storage devices. Theoretical notions here are (a) long-range and directional ET, (b) coherent and resonance electron tunneling, (c) anisotropic nuclear reorganization, (d) local mode reorganization and gated ET, and (e) molecular and mesoscopic *organization* on solid surfaces interfacing molecular function with external circuits.

Scanning tunneling (STM) and atomic force microscopy (AFM) have opened unique perspectives for mapping of molecular adsorption.[14−16] STM also offers features crucial to interfacial molecular ET. One is *functional* characterization of intermediate size molecules, in the form of spectroscopy-like relations between the tunnel current and bias voltage.[17−20] Other functional properties are the electrical potential distribution in the tunnel gap[19] and conductivity patterns via suitable HOMOs and LUMOs.[16−18,20−24] A second feature is that STM (and AFM) has been extended to the natural medium for most chemical and biological reactivity, i.e., *aqueous* solution (in situ STM/AFM). This has raised recognized issues[25−27] related to adsorbate immobilization, tip coating, independent tip and substrate potential control, and the fundamental in situ STM *phenomenon*. Electrochemically controlled in situ STM offers new spectroscopic probes based on two potential differences. In addition to the current-bias voltage relation the relation between the tunnel current and the substrate *overvoltage* relative to a reference electrode can thus be controlled. In situ STM also has the potential of imaging *dynamic* phenomena such as surface phase transitions or individual reactive events.[28,29] Still another perspective is to exploit the potentiostatic control for electrochemical manufacturing of nano- and micrometer scale turrets, holes, rectangular structures, etc.[30−32]

Adsorbate redox molecules, including redox metalloproteins, offer particular perspectives for distinction between different tunneling *mechanisms* (elastic, vibrationally assisted, etc.). They also represent fundamentals required for molecular "devices" such as current switching, rectification etc. In previous reports we have introduced the notions of tunneling and ET in three-level in situ STM, and of sequential or coherent ET.[33,34] This has revealed interesting spectroscopy-like features in the current/bias-[33−35] and /overvoltage relations.[33,34,36] In the present work we address three-level in situ STM of adsorbed redox molecules in a more systematic fashion. As in the previous reports the

* To whom correspondence should be addressed.

10.1021/jp993635x CCC: $19.00
Published on Web 11/11/2000

coupling between the redox level and the solvent or protein phonon system is strong and phonon dynamics is explicitly incorporated. We provide, however, particularly *two* new observations. One is in situ STM theory of adsorbed redox molecules in limits where one or both molecule-electrode contacts is strong and accord with *adiabatic* interfacial ET.[37] The tunnel feature then appears indirectly and the tunnel current is entirely dominated by the driving force (bias voltage or overvoltage) and redox level populations in the oxidized and reduced states. In this limit the single molecule oxidation/reduction cycle is also composed of a large number of individual ET steps transferring electrons inelastically from vibrationally unrelaxed phonon states. The other observation is that these limits give a different *interpretation* of observed in situ STM tunnel current/voltage relations distinctive from other mechanisms discussed previously.[33−36]

2. Adiabatic and Diabatic Electronic Transitions in Three-State in Situ STM Tunnel Contacts

Figure 1 shows the energy scheme for three-level ET as a basis for in situ STM.[33,34] Electron tunneling between two metallic electronic continua, representing the tip and substrate, is mediated by a molecular redox level. The electrodes are biased by the voltage V_{bias}, and the substrate potential controlled by the potential φ relative to a reference electrode. In the, initially oxidized state the level is located above both Fermi levels. Nuclear configurational fluctuations take the level close to the Fermi level of the negatively biased electrode where Landau−Zener type electronic transitions from this electrode to the molecule occur. The level subsequently initiates vibrational relaxation toward equilibrium of the reduced molecule below the Fermi levels. If the second ET step occurs *prior* to full relaxation the two steps proceed *coherently*. This limit was considered in ref 34. If, on the other hand, vibrational relaxation is achieved prior to the second ET, the latter requires renewed thermal activation, and the mechanism approaches two sequential electrochemical single-ET steps. The corresponding potential (free) energies are shown in Figure 2. Analogous considerations apply to "hole transfer" where the order of the ET steps is reversed and initiated from the *reduced* molecular level, *below* the Fermi levels. A single-channel pattern for the short-time evolution of the tunneling current could in principle be envisaged. The current would then follow vibrational relaxation across the Fermi levels in a pulselike sequence of single-channel steps. In normal STM configurations these are, however, averaged into steady-state macroscopic charge flow.

In this report we address new formal and physical schemes with focus on sequential two-channel mechanisms which extend to both the *diabatic* and *adiabatic* limits in each of the electronic transitions. Since the electronic wave function of each metallic level is normalized with respect to the whole electrode volume (box normalization), transitions involving individual levels are always strongly *diabatic*. The *adiabatic* character of the ET process is therefore rooted in multiple transitions between the electronic levels of the metal and the molecule along the potential surfaces.[1,2,38] This view can be framed by kinetic master equations. Alternatively the adiabatic interfacial ET process can be viewed as ET via adsorbed molecular levels broadened by the metallic substrate.[39−43] We consider different limits appropriate to real or putative experimental configurations.

3. Both Transitions Fully Adiabatic

In this Section we consider the limit where both ET steps are fully adiabatic. The first step is ET from levels close to the Fermi level of the negatively biased electrode to the vacant molecular level, or from the occupied molecular level to levels close to the Fermi level of the positively biased electrode. This is similar to electrochemical ET where vibrational relaxation occurs subsequently, followed by molecular diffusion out of the reaction zone. However, in the in situ STM process new electron exchange between the temporarily occupied (reduction) or vacant (oxidation) redox level and levels in the positively or negatively biased electrode, respectively, within the energy interval *between* the Fermi levels occurs *during* vibrational relaxation after the first ET (Figure 1). Multiple electronic transitions from the negatively to the positively biased electrode via the temporarily reduced molecule, while the system moves along the reaction coordinate in the forward direction, is thus a feature of the in situ STM process in the adiabatic limit. In comparison, multiple transitions in opposite directions across a single interface is a feature of *electrochemical* ET. The in situ STM current flow is thus unidirectional in a direction controlled by the bias voltage, and *both* oxidized and reduced adsorbate contribute to the current.

The formalism below refers to individual adsorbed redox molecules immobilized on the surface or monolayers of such molecules. Different current−voltage characteristics emerge in the normal, and in the activationless and inverted overvoltage ranges.

3.1. Redox Adsorbate Molecules in the Tunnel Gap. The overpotential η is defined relative to the equilibium potential of the negatively biased electrode φ_0 in such a way that the adsorbate molecules are oxidized at high *negative* η, i.e., $\eta = \varphi_0 - \varphi$. When a bias and overpotential are applied at time $t = 0$, the probabilities that the adsorbed molecule is in the oxidized Φ_{ox} or reduced form Φ_{red} evolve as

$$\Phi_{ox} = \frac{(k_{ox}/k_{red})\exp[-(k_{ox}+k_{red})t] + 1}{1 + (k_{ox}/k_{red})}$$

$$\Phi_{red} = \frac{(k_{ox}/k_{red})\{1 - \exp[-(k_{ox}+k_{red})t]\}}{1 + (k_{ox}/k_{red})} \qquad (1)$$

where k_{ox} and k_{red} are the rate constants for reduction and oxidation, respectively at given η and V_{bias}. Unlike interfacial electrochemical ET where the net current is $i = en_{ox}k_{ox}\Phi_{ox} - en_{red}k_{red}\Phi_{red}$ and decays exponentially in time, and n_{ox} and n_{red} are the number of electrons transferred in the reduction and oxidation process, respectively, *both* the oxidized and reduced molecule contribute to the in situ STM current. The observed tunnel current is

$$i_{tunn}^{ad}(t) = i_{ox}(t) + i_{red}(t) = en_{ox}k_{ox}\Phi_{ox}(t) + en_{red}k_{red}\Phi_{red}(t)$$

$$= \frac{ek_{ox}}{1 + (k_{ox}/k_{red})}\{n_{ox} + n_{red} - (n_{red} - n_{ox}k_{ox}/k_{red})\exp[-(k_{ox}+k_{red})t]\} \qquad (2)$$

The steady state is reached as $t \rightarrow \infty$, i.e.

$$i_{tunn}^{ad}(t) = e(n_{ox} + n_{red})\frac{k_{ox}k_{red}}{k_{ox} + k_{red}} \qquad (3)$$

eq 3 *resembles* a stepwise, sequential ET process but the mechanism is composed of two *different* processes. Both give unidirectional electron flow from the negatively to the positively biased electrode and are coupled by the mass balance. One process is ET via the initially oxidized adsorbate. The other

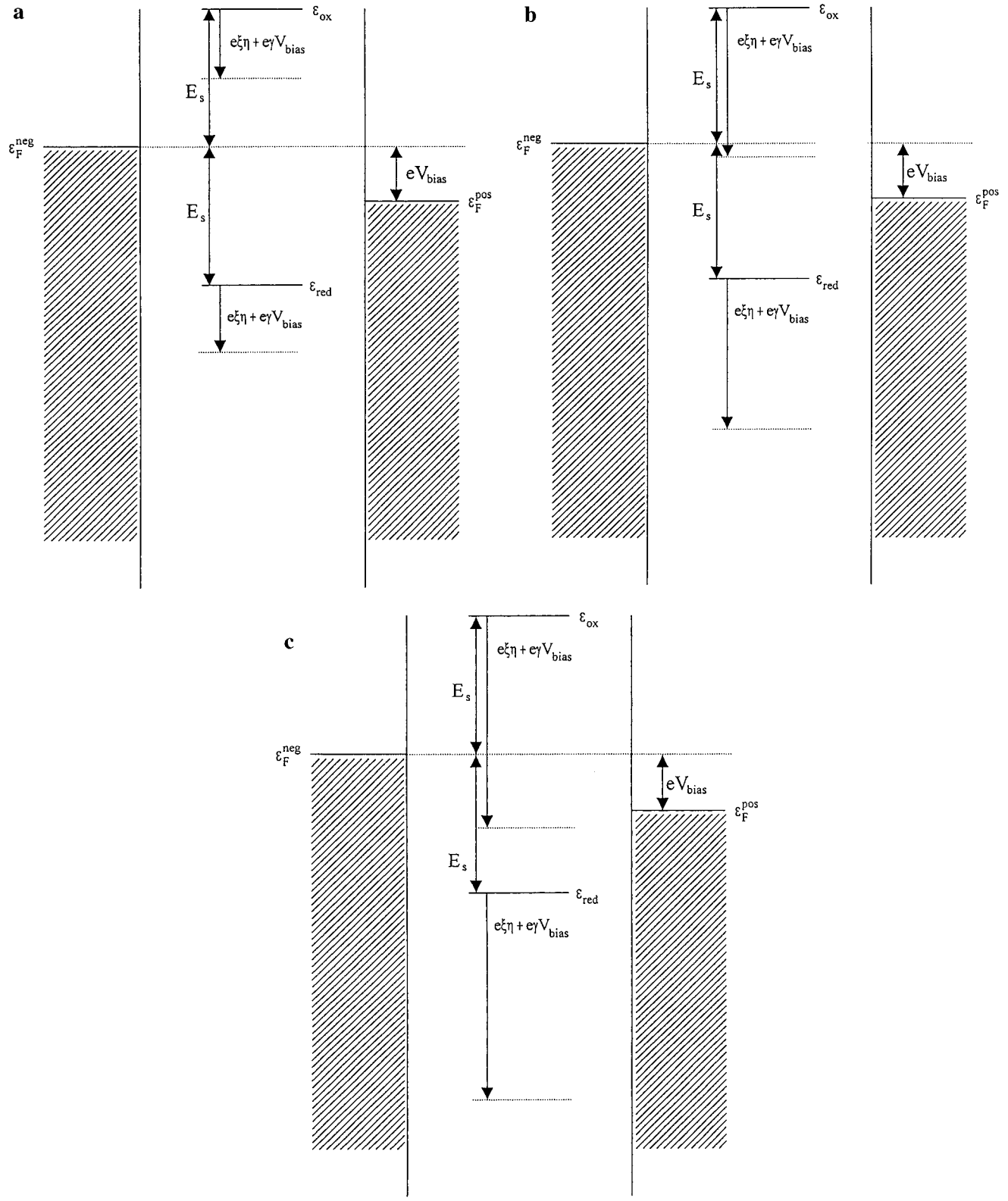

Figure 1. Electronic energy level diagram of in situ three-level electronic-vibrational STM process. The energy levels of the positively, ϵ^{pos}, and negatively biased electrode, ϵ^{neg}, are coupled via the initially vacant molecular redox level ϵ_{ox}. Fluctuations in the nuclear coordinate(s) q from $q = q_{oi}$ take the level close to the Fermi level of the negatively biased electrode, ϵ_F^{neg} where ET begins. Relaxation takes the filled molecular level towards still lower values, with full vibrational relaxation at the energy ϵ_{red} and coordinate $q = q_{red}$. ET to the positively biased electrode can occur above the Fermi level of this electrode ϵ_F^{pos} The bias voltage and the electrochemical potential variation of the redox level are shown. a: The normal overvoltage range. b: The activationless range. c: The barrierless range.

process is ET from the reduced molecular adsorbate to the positively biased electrode, followed by ET from the negatively biased electrode to the oxidized molecule. In a sense, the two processes correspond to electron and hole transfer. Electron and hole transfer thus do not need separate consideration as for coherent processes but are inherent in the approach, based on the master equations leading to eq 3 and the mass conservation condition. In short-time ranges this implies, further, that charge

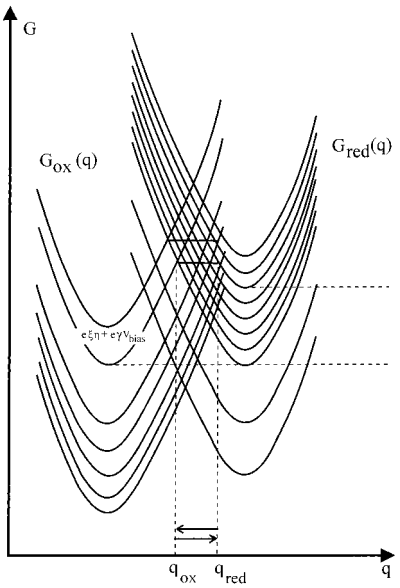

Figure 2. Nuclear potential Gibbs free energy surfaces corresponding to the electronic levels in Figure 1. The energy gap $e\xi\eta + e\gamma V_{bias}$ shows the shift of the equilibrium value of the vacant redox level at the Fermi energies of the two electrodes, caused by the bias voltage and overvoltage. The horizontal lines show adiabatic transitions from the negatively biased electrode to the molecule at zero (upper) and finite (lower) η and V_{bias}. The transition from the filled redox level to the positively biased electrode would be from the same $G_{red}(q)$-surface to $G_{ox}(q)$-surfaces around the Fermi level ϵ_F^{pos} These are lowered relative to the top $G_{red}(q)$-surface shown, by eV_{bias}.

is transferred in a pulselike fashion, by alternating reduction and oxidation steps. This could in principle hold a clue to environmental nuclear relaxation dynamics although the time resolution of present-time instrumentation is inadequate for such fast phenomena.

3.2. The Normal Overvoltage Range. In this range

$$n_{ox} = n_{red} \approx eV_{bias}/\Delta\epsilon; \quad \Delta\epsilon = \frac{1}{\kappa_{neg}\rho_{neg}} + \frac{1}{\kappa_{pos}\rho_{pos}} \qquad (4)$$

where $\Delta\epsilon$ is the metallic electronic energy level interval contributing to each single-ET step, κ the microscopic electronic transmission coefficient for a single passage of the potential surface crossing, and ρ the metallic level density. The subscripts refer to the negatively and positively biased electrode. Equation 3 can therefore be recast as

$$V_{bias}(\infty) = 2e\left(\frac{eV_{bias}}{\Delta\epsilon}\right)\frac{k_{ox}k_{red}}{k_{ox}+k_{red}} = 2e(eV_{bias})\frac{1}{(\kappa_{neg}\rho_{neg})^{-1}+(\kappa_{pos}\rho_{pos})^{-1}}\frac{k_{ox}k_{red}}{k_{ox}+k_{red}} \qquad (5)$$

Equations 4 and 5 hold two notable observations. One is that the transmission coefficients appear in the fully adiabatic limit. This is rooted in the representation of the *number* of contributing levels by the transmission coefficient (i.e., $eV_{bias}/\Delta\epsilon \propto \kappa \gg 1$) and not in current control via the transmission coefficient as in diabatic ET. The other one is that the strong electronic coupling between the redox molecule and both electrodes causes many electrons to be transferred between the electrodes in a single molecular reduction−oxidation cycle.

We shall use the following broadly valid adiabatic rate constant forms[1,2]

$$k_{ox} = \frac{\omega_{eff}}{2\pi}\exp\left[-\frac{(E_s - e\xi\eta - e\gamma V_{bias})^2}{4E_s k_B T}\right]$$

$$k_{red} = \frac{\omega_{eff}}{2\pi}\exp\left[-\frac{(E_s - eV_{bias} + e\xi\eta - e\gamma V_{bias})^2}{4E_s k_B T}\right] \qquad (6)$$

These can be extended to nuclear tunneling, mode anharmonicity, etc., as warranted. As noted, reduction and oxidation of the molecular redox level are *not* forward and reverse processes in the normal sense and the rate constants in eq 6 are not related by detailed balance conditions.

Insertion of eq 6 into eq 5 gives the steady-state tunnel current

$$i_{tunn}^{ad}(\infty) = 2e\frac{eV_{bias}}{\Delta\epsilon}\frac{\omega_{eff}}{2\pi}\times \frac{1}{\exp\left[-\frac{(E_s - e\xi\eta - e\gamma V_{bias})^2}{4E_s k_B T}\right] + \exp\left[-\frac{(E_s - eV_{bias} + e\xi\eta - e\gamma V_{bias})^2}{4E_s k_B T}\right]} \qquad (7)$$

Equation 7 holds all the features of the in situ STM system. It is illustrated in Figures 3 and 4 which prompt several observations:

(1) The tunnel current dependence of the *overvoltage* has a *maximum* at

$$\epsilon\eta = \epsilon\eta_{max} = \left(\frac{1}{2} - \gamma\right)eV_{bias}, \quad \text{or } \varphi_{max} = \varphi_0 - \frac{1}{\xi}\left[\frac{1}{2} - \gamma\right]V_{bias} \qquad (8)$$

giving the maximum current

$$i_{tunn}^{max}(\infty) = e(eV_{bias}/\Delta\epsilon)\frac{\omega_{eff}}{2\pi}\left[-\frac{\left(E_s - \frac{1}{2}eV_{bias}\right)^2}{4E_s k_B T}\right] \qquad (9)$$

The maximum is caused by variation of the activation Gibbs free energy but particularly by variation of the concentrations of the oxidized and reduced forms of the redox molecule, and the parallel variation of the two ET channels where these forms dominate. This is in contrast to adiabatic ET in homogeneous solution where the variation is caused by the activation Gibbs free energy and the transmission coefficient which assumes small values in the inverted region.

(2) The maximum is located at the equilibrium potential when the molecular redox center is exposed to half the bias potential (eq 8), and shifted when the redox site is closer to one of the electrodes. The shift is toward positive η for $\gamma < 1/2$, and positive V_{bias}, i.e., when the redox site is closest to the negatively biased electrode, or for $\gamma > 1/2$ and negative V_{bias}. It is toward negative η when $\gamma < 1/2$ and V_{bias} is negative, or $\gamma > 1/2$ and V_{bias} positive. This is different from resonance tunneling or ET in the coherent mode[34,36] where the maximum is in the activationless range, $\xi\eta \approx E_s + e\gamma V_{bias}$.

(3) The *width* of the correlation in eq 8 is

$$W = \sqrt{2\pi/|\mathrm{d}^2 \ln i_{tunn}(e\eta)/\mathrm{d}(e\eta)^2|} = k_B T E_s\sqrt{\frac{2\pi}{2k_B T E_s + (eV_{bias})^2}} \qquad (10)$$

i.e., W increases approximately as $\sqrt{k_B T E_s}$ at small bias voltages.

(4) The current decrease after the maximum is still in the *normal* overvoltage range and caused by the switch from ET

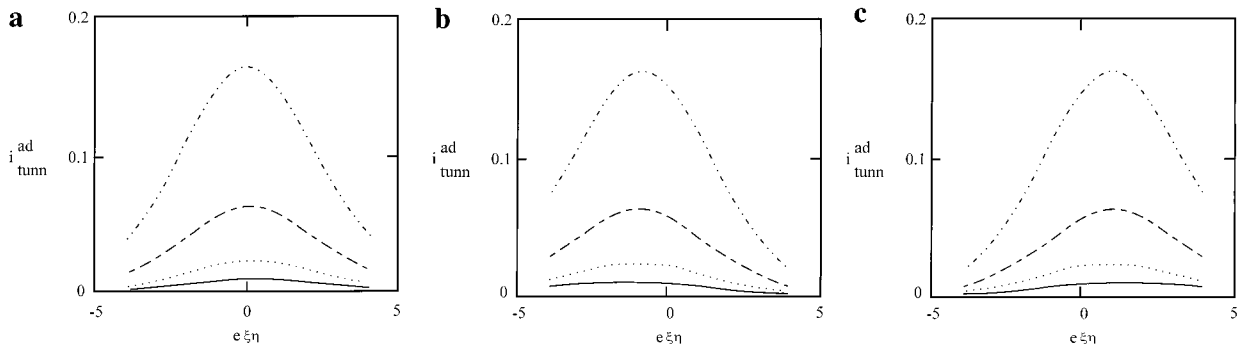

Figure 3. The dependence of the tunneling current on the overvoltage in the totally adiabatic limit calculated from eq 7. Normalized with respect to the preexponential factor. $e\xi\eta$ in units of k_BT. $eV_{bias} = 0.1$ V. The four curves represent different values of the reorganization Gibbs free energy. In units of k_BT, from top to bottom: $E_s = 8$, 12, 16, and 20. a: $\gamma = 0.5$. b: $\gamma = 0.75$. c: $\gamma = 0.25$.

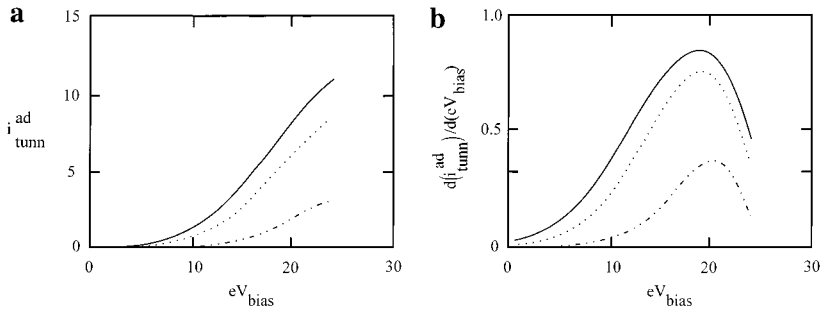

Figure 4. The dependence of the tunneling current on the bias voltage in the totally adiabatic limit calculated from eq 7. Normalized to the preexponential factor except that eV_{bias} is included in the preexponential factor. eV_{bias} and other energy quantities in units of k_BT. $\gamma = 0.5$; $E_s = 12$. From top to bottom; $e\xi\eta = 2$, 4, 8. a: The current. b: The derivative current.

predominantly via the *oxidized* adsorbate to ET predominantly via the *reduced* form ("hole transfer"). It is *not* caused by onset of the inverted overpotential region. This observation is important for experimental data interpretation (section 5).

(5) The tunnel current is finite also at negative overvoltages.

(6) The tunnel current dependence on the bias voltage, eq 7 also exhibits a structural feature of importance for data interpretation, namely, an inflection point, or a maximum in the derivative correlation (Figure 4). The inflection point is at a lower bias potential than the values which would bring the redox level to traverse the Fermi level of the negatively biased electrode, i.e., $e\gamma V_{bias} \approx E_s + |e\xi\eta|$ where inflection appears in single-channel mechanisms. In the mechanism presently addressed ET from the reduced redox level begins to operate at smaller bias voltage and the inflection also appears earlier.

(7) In the limit where each step is controlled by solvent relaxation, and stochastic effects become important, an interesting difference from adiabatic single-step electrochemical ET emerges. In the latter case $\omega_{eff}/2\pi$ in the preexponential factor of the rate constant follows a τ_L^{-1} or ζ^{-1} dependence where τ_L is the longitudinal relaxation time and ζ the viscosity. On the other hand, the number of individual level transitions at the second electrode in the in situ STM configuration, i.e., $\approx \rho_{pos}eV_{bias}$, is modified in the stochastic limit approximately by the factor l_{TS}/λ where l_{TS} is the extension of the region between q_{0i} and q_{red} (Figure 2) and λ the mean free path for diffusive barrier crossing. λ is approximately $\lambda \approx (2\mu k_BT)^{1/2}/\zeta$ [44] where μ is the effective mass for motion along the nuclear coordinate. The preexponential factor in eq 7 is therefore modified by an additional factor proportional to ζ, giving overall friction independence in the solvent controlled adiabatic limit.

3.3. The Activationless and Inverted Overvoltage Regions. Application of large overvoltages lowers the vacant molecular redox level to a position between the two Fermi levels. This accords with the activationless and inverted overvoltage regions and converts the initially oxidized molecule to the reduced form. The tunnel current, at zero time, is

$$i^{act.l}_{tunn}(0) = en_{ox}k^{act.l}_{ox} \tag{11}$$

with the steady-state value

$$i^{act.l}_{tunn}(\infty) = e(n_{ox} + n_{red})k_{red} = e(n_{ox} + n_{red})\frac{\omega_{eff}}{2\pi}\exp\left[-\frac{(E_s - eV_{bias} + e\xi\eta - e\gamma V_{bias})^2}{4E_sk_BT}\right] \tag{12}$$

since $k_{ox} \gg k_{red}$. The overall process is, however, dominated by ET from the reduced molecule since also $\Phi_{red} \gg \Phi_{ox}$. In this region, $E_s > eV_{bias}$ and the steady-state current *decreases* with *increasing* overpotential. In addition, the following applies

$$n_{ox} = n_{red} \approx (eV_{bias} + E_s - e\xi\eta - e\gamma V_{bias})/[(k_{red}\rho_{red})^{-1} + (k_{ox}\rho_{ox})^{-1}] \tag{13}$$

The steady-state tunnel current in this overpotential range is therefore composed of formally *activationless* reduction from the negatively biased electrode and *barrierless* reoxidation of the reduced molecule by the positively biased electrode. The barrierless feature dominates but only follows patterns for barrierless electrochemical single-step ET when there is no barrier for the second transition (Figure 1). The current/overpotential relation is also different and the symmetry factor in the barrierless region is no longer unity such as for barrierless electrochemical ET.

The "inverted" overpotential range is reached when the overpotential is so high that the vacant molecular level is initially

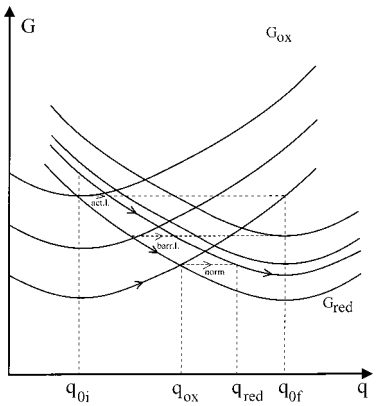

Figure 5. ET transitions along the nuclear reaction coordinate q from the initial, q_{0i} to the final equilibrium configuration q_{0f}. "Normal", activationless, and barrierless overvoltage ranges are shown.

(i.e., $t = 0$) *below* both Fermi levels. No tunnel current flows in this level configuration. As the molecular level is, however, rapidly converted to the relaxed *reduced* form, a small steady-state current from the reduced level to the positively biased electrode ("hole transfer") still flows. This current accords with the notion of "inverted region". Unlike the common use of this concept where the inverted region follows the *activationless* region, this region follows here the *barrierless* region. The tunnel current is

$$i_{\text{tunn}}^{\text{ad}} = e(n_{\text{ox}} + n_{\text{red}})\frac{\omega_{\text{eff}}}{2\pi}\exp\left[-\frac{(E_s - eV_{\text{bias}} + e\xi\eta - e\gamma V_{\text{bias}})^2}{4E_s k_B T}\right] \quad (14)$$

i.e., as eq 12 but $n_{\text{ox}} = n_{\text{red}} \approx (2k_B T/\alpha)/[(k_{\text{neg}}\rho_{\text{neg}})^{-1} + (k_{\text{pos}}\rho_{\text{pos}})^{-1}]$, independent of η.

3.4. Coherent Adiabatic Tunneling Currents and Highly Asymmetric Barriers. An inherent assumption in eqs 5−10 is that the bias voltage is small compared to the reorganization Gibbs free energy E_s/e and that the system is electronically approximately symmetric, i.e., $\kappa_{\text{neg}}\rho_{\text{neg}} \approx \kappa_{\text{pos}}\rho_{\text{pos}}$. The effective potential barriers (Figure 5) are then practically constant over the whole transition region, and all trajectories with energies above $G(q_{\text{ox}})$ or $G(q_{\text{red}})$ contribute to the reduction/oxidation cycle. New features appear in cases of high asymmetry resulting particularly from different electron coupling of the redox level with the electrode and the tip, or from large bias voltages, i.e., $eV_{\text{bias}} > E_s$. We consider first a nonsymmetric system at small bias voltage. The effective potential $G_{\text{eff}}(q)$ then in general either increases or decreases in the region between q_{ox} and q_{red} reaching the highest value at q_{red} and q_{ox}, respectively. The system must overcome this barrier for reduction or oxidation to occur, and these reactive trajectories contribute to the tunneling current rather similarly to the mechanism for symmetric barriers. Trajectories with energies lower than this barrier height may be denoted as *nonreactive* since they do not result in oxidation or reduction of the redox level and return to the states from which they originated. Some of them may, however, still contribute to the tunneling current in a competitive coherent but "nonreactive"channel, $i_{\text{non-r}}^{\text{ad}}$. When the effective nuclear potential increases in the region between q_{ox} and q_{red} these trajectories start from the oxidized state with energies higher than $G_{\text{eff}}(q_{\text{ox}})$. The trajectories start from the reduced state with energies higher than $G_{\text{eff}}(q_{\text{red}})$ when the potential decreases in the region between q_{ox} and q_{red}. In either case the nonreactive trajectories temporarily bring the redox level into the energy region between the two Fermi levels for a short time determined by the characteristic time scale for motion along the reaction coordinate q. The total current in the adiabatic limit is thus

$$i = i_{\text{tunn}}^{\text{ad}} + i_{\text{non-r}}^{\text{ad}} \quad (15)$$

The barrier shape and tunneling mechanisms at high bias voltage can be addressed in greater detail by the following consideration. $i_{\text{tunn}}^{\text{ad}}$ is still represented by eq 3 but with dfferent activation Gibbs free energies and transmission coefficients. The effective potential $G_{\text{eff}}(q)$, and hence, $G(q_{\text{ox}})$ and $G(q_{\text{red}})$ can be obtained most conveniently from[45]

$$G_{\text{eff}}(q) = \frac{1}{2}\hbar\omega(q - q_{0i})^2 - \int_{q_{0i}}^{q} dq\sqrt{2E_s\hbar\omega}\langle n(q)\rangle \quad (16)$$

where harmonic motion along q with the frequency ω is assumed. $2\pi h$ is Planck's constant and $\langle n(q)\rangle$ the average redox level population. $\langle n(q)\rangle$ is approximately

$$\langle n\rangle = \frac{k_{\text{neg}}\rho_{\text{neg}}}{k_{\text{neg}}\rho_{\text{neg}} + k_{\text{pos}}\rho_{\text{pos}}} \quad (17)$$

in the q range $q_{\text{ox}} < q < q_{\text{red}}$, i.e., independent of q. If

$$G(q_{\text{ox}}) > G(q_{\text{red}}), \quad \text{or } 2\xi\eta - (1 - 2\gamma)eV_{\text{bias}} > 2E_s(1 - \langle n\rangle) \quad (18)$$

then

$$k_{\text{ox}} = \frac{\omega_{eff}}{2\pi}\exp\left[-\frac{(E_s - e\xi\eta - e\gamma V_{\text{bias}})^2}{4E_s k_B T}\right];$$

$$k_{\text{red}} = k_{\text{ox}}\exp\left[-\frac{e\xi\eta - e\gamma V_{\text{bias}} + V_{\text{bias}}(1 - \langle n\rangle)^2}{k_B T}\right]$$

$$i_{\text{non-r}}^{\text{ad}} = \frac{k_{\text{ox}}}{k_{\text{red}} + k_{\text{ox}}}\frac{2\sqrt{\pi E_s k_B T}}{\Delta\epsilon}\frac{\omega_{eff}}{2\pi}\exp\left[-\frac{G(q_{\text{red}}) - G(q_{0f})}{k_B T}\right] =$$

$$i_{\text{non-r}}^{\text{ad}} = \frac{k_{\text{ox}}k_{\text{red}}}{k_{\text{red}} + k_{\text{ox}}}\frac{2\sqrt{\pi E_s k_B T}}{\Delta\epsilon}\frac{\omega_{eff}}{2\pi}\exp\left[-\frac{G(q_{\text{ox}}) - G(q_{\text{red}})}{k_B T}\right] =$$

$$G(q_{\text{red}}) - G(q_{\text{ox}}) = \frac{(eV_{\text{bias}})^2}{4E_s} + \frac{eV_{\text{bias}}}{2E}[E_s(1 - 2\langle n\rangle) - e\xi\eta - e\gamma V_{\text{bias}}] \quad (19)$$

When the inverse condition applies the rate constants and tunneling currents become

$$k_{\text{ox}} = \frac{\omega_{\text{eff}}}{2\pi}\exp\left[-\frac{(E_s - e\xi\eta - e\gamma V_{\text{bias}} + eV_{\text{bias}})^2}{4E_s k_B T}\right] + \frac{eV_{\text{bias}}\langle n\rangle}{k_B T}$$

$$k_{\text{red}} = \frac{\omega_{\text{eff}}}{2\pi}\exp\left[-\frac{(E_s - e\xi\eta - e\gamma V_{\text{bias}} + eV_{\text{bias}})^2}{4E_s k_B T}\right] \quad (20)$$

giving

$$i_{\text{non-r}}^{\text{ad}} = \frac{k_{\text{red}}}{k_{\text{red}}+k_{\text{ox}}}\frac{\omega_{\text{eff}}}{2\pi}\frac{2\sqrt{\pi E_s k_B T}}{\Delta\epsilon}\exp\left[-\frac{G(q_{\text{ox}})-G(q_{0f})}{k_B T}\right] = \frac{2\sqrt{\pi E_s k_B T}}{\Delta\epsilon}\frac{k_{\text{red}}k_{\text{ox}}}{k_{\text{red}}+k_{\text{ox}}}\exp\left[\frac{G(q_{\text{red}})-G(q_{\text{ox}})}{k_B T}\right] \quad (21)$$

where $G(q_{\text{ox}}) - G(q_{\text{red}})$ is given by eq 19 and $\Delta\epsilon$ by eq 4.

Equations 19 and 20 represent the vibrationally coherent nonreactive channel, with no vibrational relaxation in the q-region between $G(q_{\text{ox}})$ and $G(q_{\text{red}})$. Nonreactive contributions with vibrational relaxation are important when the equilibrated reduced molecular level is brought between ϵ_F^{neg} and ϵ_F^{pos}, by a high bias voltage, $eV_{\text{bias}} > E_s$. The effective potential can then even have a minimum in the region between q_{ox} and q_{red} and the coherently mediated current is entirely determined by partially populated relaxed redox level states with energies between the two Fermi levels, i.e.,

$$i_{\text{non-r}}^{\text{ad}} = \frac{eC}{\tau};\quad C = \frac{k_{\text{ox}}k_{\text{red}}}{k_{\text{red}}+k_{\text{ox}}};\quad \tau = \tau_{\text{neg}}+\tau_{\text{pos}} \quad (22)$$

where times for electron exchange and level broadening factors have been introduced

$$\tau_{\text{neg}} = \frac{\hbar}{\Delta_{\text{neg}}};\quad \tau_{\text{pos}} = \frac{\hbar}{\Delta_{\text{neg}}}$$

$$\Delta_{\text{neg}} = \pi(V_{\text{neg}})^2\rho_{\text{neg}};\quad \Delta_{\text{pos}} = \pi(V_{\text{neg}})^2\rho_{\text{pos}} \quad (23)$$

giving the following form to $i_{\text{non-r}}^{\text{ad}}$

$$i_{\text{non-r}}^{\text{ad}} \approx \frac{k_{\text{ox}}k_{\text{red}}}{k_{\text{red}}+k_{\text{ox}}}\frac{e\Delta}{\hbar};\quad \Delta^{-1} = \Delta_{\text{neg}}^{-1}+\Delta_{\text{pos}}^{-1} \quad (24)$$

where V_{neg} and V_{pos} are the electron exchange integrals coupling the redox level with the negatively and positively biased electrode, respectively. The rate constants are given by eqs 19−21. Starting with an initially oxidized level, the current then first rises with increasing overvoltage until the region near the equilibrium potential. This is followed by a (wide) range ($\approx V_{\text{bias}}$) of approximately constant tunneling current, $i_{\text{non-r}}^{\text{ad}} \approx e\Delta/\hbar$, mediated largely by the partially reduced molecule. $i_{\text{non-r}}^{\text{ad}}$ only begins to decrease when the overvoltage takes such large values that the equilibrated reduced molecular level is lowered *below* ϵ_F^{pos}. This is clearly different both from the behavior of $i_{\text{tunn}}^{\text{ad}}$ and of $i_{\text{non-r}}^{\text{ad}}$ at small bias voltage where much sharper maxima in the current/overvoltage relation are expected.

4. Partially Adiabatic Transitions

This limit applies when the redox center is significantly closer to one of the electrodes than to the other one. Adsorbed redox metalloproteins, to which in situ STM has recently been extended,[46−50] could be such examples where the strongly asymmetric location of the metal for example in cytochromes and blue single-copper proteins implies that the electronic contacts with the two metallic electrodes are different

We consider specifically the limit where the negatively biased electrode is strongly coupled to the redox level while coupling to the positively biased electrode is weak,

$$\kappa_{\text{neg}}\rho_{\text{neg}}k_B T \approx 1;\quad \kappa_{\text{neg}}\rho_{\text{neg}}k_B T \ll 1 \quad (25)$$

The same formalism, particularly eq 7, as in the previous section, applies again but the widely different transmission coefficients now endow the process with new features.

We assume that electron exchange at the negatively biased electrode is fast enough that equilibrium at this electrode is established. The equilibrium populations of the oxidized and reduced forms of the molecule are then

$$\Phi_{\text{red}} = \frac{k_{\text{red}}^{\text{neg}}/k_{\text{ox}}^{\text{neg}}}{1+(k_{\text{red}}^{\text{neg}}/k_{\text{ox}}^{\text{neg}})};\quad \Phi_{\text{ox}} = \frac{1}{1+(k_{\text{red}}^{\text{neg}}/k_{\text{ox}}^{\text{neg}})}$$

$$k_{\text{red}}^{\text{neg}}/k_{\text{ox}}^{\text{neg}} = \exp\left[\frac{e\xi\eta - e\gamma V_{\text{bias}}}{k_B T}\right] \quad (26)$$

The subscript refers to electron exchange between the reduced or oxidized molecule and the negatively biased electrode. The tunnel current is

$$i_{\text{tunn}}^{\text{p.ad}} = \kappa_{\text{pos}}\frac{\omega_{\text{eff}}}{2\pi}\rho_{\text{pos}}\left\{(eV_{\text{bias}})\frac{\exp\left[-\frac{e\xi\eta+e\gamma V_{\text{bias}}}{4E_s k_B T}\right]}{1+\exp\left[-\frac{e\xi\eta+e\gamma V_{\text{bias}}}{k_B T}\right]}\times \exp\left[-\frac{(E_s - e\xi\eta - e\gamma V_{\text{bias}})^2}{4E_s k_B T}\right] + (2k_B T/\alpha)\frac{1}{1+\exp\left[-\frac{e\xi\eta+e\gamma V_{\text{bias}}}{k_B T}\right]}\times \exp\left[-\frac{(E_s - eV_{\text{bias}} + e\xi\eta + e\gamma V_{\text{bias}})^2}{4E_s k_B T}\right]\right\} \quad (27)$$

The first term in eq 27 represents ET from the initially vacant redox level to the positively biased electrode after this level has become temporarily occupied. The second term represents ET from the initially occupied redox level to the positively biased electrode, followed by fast ET from the negatively biased electrode to the vacant redox level. The factors (eV_{bias}) and $(2k_B T/\alpha)$ are the metallic electronic level ranges contributing to the two steps.

The reverse case of eq 25

$$\kappa_{\text{neg}}\kappa_{\text{neg}}k_B T \ll 1;\quad \kappa_{\text{pos}}\kappa_{\text{pos}}k_B T \approx 1 \quad (28)$$

follows the same formalism, with the subscripts "neg" and "pos" reversed. There is now equilibrium with the positively biased electrode, with the equilibrium constant

$$\frac{\Phi_{\text{ox}}}{\Phi_{\text{red}}} = \frac{k_{\text{red}}^{\text{pos}}}{k_{\text{ox}}^{\text{pos}}} = \exp\left[\frac{e\xi\eta + e\gamma V_{\text{bias}} - eV_{\text{bias}}}{k_B T}\right] \quad (29)$$

giving the tunnel current

$$i_{\text{tunn}}^{\text{p.ad}} = \kappa_{\text{neg}}\frac{\omega_{\text{eff}}}{2\pi}\rho_{\text{neg}}\left\{(2k_{\text{B}}T/\alpha)\frac{\exp\left[\frac{e\xi\eta + e\gamma V_{\text{bias}} - eV_{\text{bias}}}{k_{\text{B}}T}\right]}{1+\exp\left[\frac{e\xi\eta + e\gamma V_{\text{bias}} - eV_{\text{bias}}}{k_{\text{B}}T}\right]}\times \exp\left[-\frac{(E_{\text{s}} - e\xi\eta - e\gamma V_{\text{bias}})^2}{4E_{\text{s}}k_{\text{B}}T}\right] + (eV_{\text{bias}})\frac{1}{1+\exp\left[-\frac{e\xi\eta + e\gamma V_{\text{bias}} - eV_{\text{bias}}}{k_{\text{B}}T}\right]}\times \exp\left[-\frac{(E_{\text{s}} - eV_{\text{bias}} + e\xi\eta + e\gamma V_{\text{bias}})^2}{4E_{\text{s}}k_{\text{B}}T}\right]\right\} \quad (30)$$

The maximum is at negative η for eq 27 and at positive η for eq 30. Equations 27 and 30 exhibit a behavior different from the fully adiabatic limit. When electron exchange with the negatively biased electrode is fast, this step is equilibrated and the second step rate determining. When electron exchange with the positively biased electrode is fast the first ET step is rate determining, followed by the fast second step. The different rate constants are also reflected in "asymmetry" in the current/overvoltage relation (Figure 6). Both equations exhibit a maximum which is, however, shifted from zero to positive η for $\kappa_{\text{neg}} \ll \kappa_{\text{pos}}$ (eq 30) and to negative η for $\kappa_{\text{neg}} \gg \kappa_{\text{pos}}$ (eq 27).

5. Totally Diabatic Transitions

This limit was considered in our previous reports[33,34] where single-channel electron and hole transfer were in focus. In the strongly diabatic limit the small tunnel factors are likely to slow the second ET so that complete intermediate (reduced) state vibrational relaxation is reached. The process is then composed of two sequential, independent diabatic electrochemical single-step reactions.

The mass balance for sequential two-step ET is

$$\frac{d\Phi_{\text{ox}}}{dt} = -\frac{d\Phi_{\text{red}}}{dt} = -\vec{k}_{\text{ox}}\Phi_{\text{ox}} + (\vec{k}_{\text{red}} + \overleftarrow{k}_{\text{red}})\Phi_{\text{red}} \quad (31)$$

the arrows "$\rightarrow$" and "$\leftarrow$" denote ET from the negatively to the positively biased electrode and in the opposite direction, respectively. The reverse direction is important in view of the small values of the rate constants in the strongly diabatic limit. In the steady state

$$\Phi_{\text{ox}} = \frac{\vec{k}_{\text{red}} + \overleftarrow{k}_{\text{red}}}{\vec{k}_{\text{ox}} + \vec{k}_{\text{red}} + \overleftarrow{k}_{\text{red}}}; \quad \Phi_{\text{red}} = \frac{\vec{k}_{\text{ox}}}{\vec{k}_{\text{ox}} + \vec{k}_{\text{red}} + \overleftarrow{k}_{\text{red}}} \quad (32)$$

The unidirectional current flow from the negatively to the positively biased electrode is

$$i_{\text{tunn,seq}}^{\text{dia}} = e\vec{k}_{\text{red}}\Phi_{\text{ox}} = \frac{\vec{k}_{\text{ox}}\vec{k}_{\text{red}}}{\vec{k}_{\text{ox}} + \vec{k}_{\text{red}} + \overleftarrow{k}_{\text{red}}} \quad (33)$$

The total current also holds a coherent two-step channel.[34] The contribution from this channel $i_{\text{tunn,seq}}^{\text{dia}}$ is important for *weakly* diabatic processes but not competitive against sequential two-step ET in the *strongly* diabatic limit (see, however, below). The diabatic two-step tunnel current is then

$$i_{\text{tunn}}^{\text{dia}} = i_{\text{tunn,seq}}^{\text{dia}} + i_{\text{tunn,coh}}^{\text{dia}} = e\vec{k}_{\text{red}}\Phi_{\text{red}} + ek_{\text{ox}}^{\text{coh}}\Phi_{\text{ox}} = e\frac{\vec{k}_{\text{ox}}\vec{k}_{\text{red}} + (\vec{k}_{\text{red}} + \overleftarrow{k}_{\text{red}})k_{\text{ox}}^{\text{coh}}}{\vec{k}_{\text{ox}} + \vec{k}_{\text{red}} + \overleftarrow{k}_{\text{red}}} \quad (34)$$

$k_{\text{ox}}^{\text{coh}}$ was analyzed previously[34] and will be disregarded presently. Equation 33 is then the formal tunnel current in the strongly diabatic limit. The three rate constants are

$$\vec{k}_{\text{ox}} = \kappa_{\text{neg}}\rho_{\text{neg}}\frac{\omega_{\text{eff}}}{2\pi}\left(\frac{2k_{\text{B}}T}{\alpha_{\text{neg}}}\right)\exp\left[-\frac{(E_{\text{s}} - e\xi\eta - e\gamma V_{\text{bias}})^2}{4E_{\text{s}}k_{\text{B}}T}\right]$$

$$\vec{k}_{\text{red}} = \kappa_{\text{pos}}\rho_{\text{pos}}\frac{\omega_{\text{eff}}}{2\pi}\left(\frac{2k_{\text{B}}T}{\alpha_{\text{pos}}}\right)\exp\left[-\frac{(E_{\text{s}} - eV_{\text{bias}} + e\xi\eta + e\gamma V_{\text{bias}})^2}{4E_{\text{s}}k_{\text{B}}T}\right]$$

$$\overleftarrow{k}_{\text{red}} = \vec{k}_{\text{ox}}\exp\left[-\frac{e\xi\eta + e\gamma V_{\text{bias}}}{k_{\text{B}}T}\right] \quad (35)$$

$\vec{k}_{\text{ox}}$, $\vec{k}_{\text{red}}$, and $\overleftarrow{k}_{\text{red}}$ are also the rate constants for diabatic electrochemical single-step processes. The subscripts "neg" and "pos" indicates that the transfer coefficients are different at the negatively and positively biased electrodes.

Formally similar tunnel currents apply in the activationless overpotential range. $\vec{k}_{\text{ox}}$ and $\overleftarrow{k}_{\text{red}}$ are then replaced by the activationless and barrierless limit, respectively, of the electrochemical single-step current while $\vec{k}_{\text{red}}$ is in the normal range. The coherent two-step mode is now more likely to be competitive because $\vec{k}_{\text{red}}$ is thermally activated in the sequential mode whereas the second step in the coherent two-step mode is activationless. The latter is thus competitive despite its smaller tunnel factor. Similar considerations apply to the inverted range where coherent two-step ET has a smaller activation Gibbs free energy in the second step than the fully relaxed $\vec{k}_{\text{red}}$ term, and $k_{\text{ox}}^{\text{coh}}$ is therefore competitive. Figure 6 shows the voltage dependences of the diabatic sequential two-step tunnel current with a single maximum in the overvoltage dependence. This is in contrast to the view of the diabatic tunnel process as two independent single-channel modes[34] where separate maxima for electron and hole transfer appear. The maximum is shifted with the tunnel factors at the two electrodes.

6. Discussion: STM Patterns of Adsorbed and Covalently Immobilized Redox Metalloproteins and Metalloporphyrins

We have provided an analytical formalism for electrochemical in situ STM of adsorbed redox molecules which are temporarily reduced or oxidized as part of the tunnel current flow between the tip and the substrate. Focus was on the limit where the tunnel process can be viewed as two consecutive equilibrated ET processes. Fully adiabatic, partially adiabatic, and fully diabatic limits have been considered, and the effect of bias voltage and overvoltage variation illustrated. The results clearly extend previous approaches to STM of redox molecules. Approaches in refs 34 and 36 addressed coherent, i.e., vibrationally unrelaxed two-step, and strictly three-level resonant mechanisms, respectively. The electrochemical in situ STM configuration was considered explicitly in both reports but the resonant and coherent mechanisms are clearly distinct from the sequential two-step formalism in the present report. Sequential two-step ET in the context of in situ STM was first introduced in ref 33 but without numerical illustrations of current−voltage spectroscopy. Such illustrations were provided in ref 35 the formalism of which rests heavily on refs 33b,c. A new feature

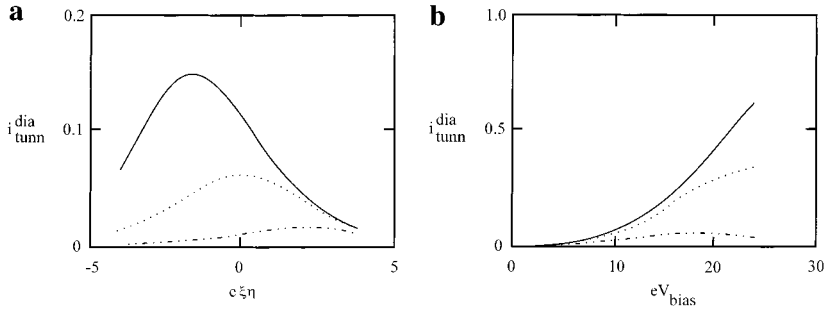

Figure 6. The dependence of the tunneling current on the overvoltage and bias voltage in the totally diabatic limit, calculated from eqs 31 and 33. The preexponential factors except the electronic transmission coefficients disregarded. Energy quantities in units of k_BT. $\gamma = 0.5$; $E_s = 12$. The ratio between the transmission coefficients of the negatively and positively bias electrode denoted as p. a: The dependence on the overvoltage. $eV_{bias} = 0.1$ V. b: The dependence on the bias voltage. $e\xi\eta = 0.1$ V. From top to bottom; $p = 0.1$, 1, 10.

was the addition of an internal high-frequency nuclear mode which opens new tunneling current channels as the bias voltage is raised and the internal mode vibrationally excited. Reference 35, however, addresses solely ex situ STM without control of the electrochemical potentials of the working electrode and the tip. In addition, the consideration was confined to the diabatic limit.

The present report covers all the cases of fully and partially adiabatic transitions as well as the fully diabatic limit and discloses spectroscopic current−bias voltage and spectroscopic current−overvoltage features. In addition, new features of the two-step process have been disclosed, particularly transparent in the fully adiabatic limit. The combined cycle of molecular reduction and oxidation is, first, shown to be composed of large numbers ($\approx eV_{bias}\kappa\rho$) of individual interfacial ET events between the molecular level and both electrodes, as the molecular level relaxes between the two Fermi levels. This enhances tunneling well above the single-ET level. The overall process has, second, a pulselike character where charge is transferred in a stepwise fashion in each reduction/oxidation cycle. This bears some resemblance to Coulomb blockade and reflects environmental nuclear relaxation at short time scales. In steady-state STM currents these effects are, however, entirely eroded. The report addresses, third, the activationless and inverted overvoltage ranges which take entirely different forms compared with resonance and coherent two-step in situ STM processes. The formalism can, fourth, be brought to incorporate straightforwardly other features such as high-frequency nuclear modes and nuclear tunneling, by established procedures.[1,2] This would add fine structure to the current−bias voltage and current−overvoltage relations reminiscent of spectroscopic vibrational fine-structure. Equations 7, 12, 14, 27, 30, 34, and 35 apply, finally, equally when the bias voltage is reversed if the quantities $\xi\eta$ and γ are replaced by $\xi\eta + V_{bias}$ and $-\gamma$, respectively. For example, the fully adiabatic tunnel current then differs from eq 7 solely by the sign of the two $e\xi\eta$-terms while eqs 8 and 9 remain unchanged.

The two-step mechanism can sustain significant tunneling currents. As an illustration, in the normal current−overvoltage region the activation Gibbs free energy in eq 6 varies from $\approx {}^1/_4E_s$ to zero at small bias voltage. Two-step tunneling would also often be controlled by the slower of the two single-ET steps. Combination of eq 6 with eq 7 gives a tunneling current for adiabatic single-ET of ≈20 nA in the activationless overvoltage region and of 1−3 nA close to the equilibrium potential, if ω_{eff} is $10^{11}-10^{12}$ s^{-1} and $E_s = 0.2-0.3$ eV. The values are even larger when the multi-ET character of the fully adiabatic process is considered. The currents are of course smaller in the partially adiabatic and totally diabatic limits but still in ranges common in experimental investigations. Sequential two-step ET was also noted to be broadly competitive with coherent two-step tunneling. This is because the diabatic rate constants of the latter hold two tunneling factors, and the former commonly only one. The coherent two-step mechanism gains importance as the electronic coupling approaches the adiabatic limit and the overpotential is shifted to the activationless and inverted overpotential regions.

The formalism is a frame for observable spectroscopy-like relations between the tunnel current and the bias or overvoltage. Such relations provide a distinction between different tunneling *mechanisms* but suitable data are rare. Lee et al. reported STM current−bias voltage relations of immobilized bare and platinized photosystem I reaction centers.[18] These contain several redox centers which could be populated in the ±1 V bias voltage range used. Imaging was ex situ but the centers are coupled to an almost continuous distribution of environmental nuclear modes in the protein. The data showed semiconductor or diode-like behavior depending on the degree of metallization but were not conclusive as to the role of the biological ET centers. Snyder and White found symmetric ex situ STM current−bias voltage relations of multilayers of Fe-protoporphyrin IX (FPP) on highly oriented pyrolytic graphite (HOPG).[51] The data were interpreted in terms of tunneling via the adsorbate metal centers. The current could be converted to a (composite in view of the multilayer nature of the adsorbate) rate constant which followed a bias voltage dependence qualitatively resembling expectations from ET theory[1,2] but without the notion of overvoltage. The large values of the rate constants ($10^9-5 \times 10^{10}$ s^{-1}) and the approach to activationless behavior at high bias voltages are notable.

Other recent studies have a bearing on the results of the present study. Molecular resolution was achieved[48−50] in studies of the blue single-copper redox protein azurin adsorbed on Au(111) in the electrochemical in situ STM mode.[48−50] This molecule is suited for adsorption via a disulfide group in the protein surface. A submolecular feature was assigned to tunneling enhancement via the copper atom,[49] but the tunnel current dependence on the bias voltage and overvoltage was weak. A reason for this could be that a large bias voltage had to be used, i.e., ≈ 0.4 V. This could bring the equilibrated filled redox level in to a position between the two Fermi levels, with opening of coherent channels, cf. Section 3.4.

Lindsay, Tao, and their associates reported current−bias voltage relations of several metalloporphyrins covalently immobilized on Au(111) in mesitylene solution.[52] These data illuminate other features but were not recorded under electrochemical potential control. Metal-specific redox behavior was disclosed, with broad derivative current/bias voltage peaks at large negative bias voltages (cf. Figures 4−6). *Distributions* of peak potentials and widths were also found on successive single-molecule scanning, with possible bearings on stochastic single-molecule features. The analysis in ref 52 rested on the notion of a parametric formal potential of the adsorbed metalloporphyrins. As the rerganization Gibbs free energy is likely to be small, i.e., 0.2−0.3 eV[34,53] the formalism above could then

suggest the following: (a) The potential parameter is close to zero and the fraction of the bias potential drop at the redox site γ, about 0.4. This would give a peak at approximately the observed position if both ET steps are either fully adiabaic or fully diabatic with roughy equal tunneling factors. (b) Partially adiabatic behavior could prevail, with ET between substrate and adsorbate likely to be a diabatic transition. This would shift the maximum toward negative values (Figure 6) and give a larger γ. (c) A finite negative potential parameter would increase γ to values between 0.5 and unity. This could also accord with the different interactions between the metalloporphyrins and the two electrodes.

The data of Tao[53] who reported tunneling current−overvoltage relations for iron protoporphyrin IX monolayers on HOPG, provide a well characterized target for quite accurate data analysis. The tunneling current shows a maximum close to the equilibrium oxidation−reduction potential, with a 4-fold apparent height variation (in the constant current mode) and a width of $\approx$ 0.3 V. Resonance tunneling[54] and coherent single-channel two-step ET[34] have been assigned as mechanisms formally in keeping with an observed maximum. Both of these mechanisms, however, require that the maximum is shifted from the equilibium potential approximately by the reorganization Gibbs free energy, ($\approx$0.2 eV). Reservations as to the reference electrode potential have been expressed.[54] Other reservations could apply to the electrochemical potential distribution in the tunnel gap. We note, however, that a maximum in the tunnel current−overvoltage relation around the equilibrium potential is fully in keeping with the sequential two-channel mechanisms discussed in the present work and a bias potential drop at the site of the redox center close to half of the total potential drop. This conclusion applies to both the fully adiabatic and fully diabatic limits and accords with the voltammetry of iron protoporphyrin IX on HOPG. Adiabatic sequential ET is, moreover, competitive with resonance and coherent two-step mechanisms as the current is not attenuated by electronic tunneling in this limit. While, according to ref 54 the issue of the reference potential is perhaps open, the present investigation illuminates the mechanistically diagnostic value of the theoretical frames and the need for unprejudiced consideration of more than a single tunneling mechanism.

Acknowledgment. Financial support from the Danish Technical Science Research Council, The Carlsberg and Novo Nordisk Foundations, The Russian Foundation for Basic Research (Grant 00-03-32239), and the EU program INTAS (Project 1093) is acknowledged.

References and Notes

(1) Kuznetsov, A. M. *Charge Transfer in Physics, Chemistry, and Biology*; Gordon & Breach: Amsterdam, 1995.
(2) Kuznetsov, A. M.; Ulstrup, J. *Electron Transfer in Chemistry and Biology. An Introduction to the Theory*; Wiley: Chichester, 1999.
(3) Marcus, R. A.; Sutin, N. Biochim. *Biophys. Acta* **1985**, *811*, 265−322.
(4) *Chem. Rev.* **1992**, *92*, 385−49 (Special Section on Electron Transfer).
(5) *Chem. Phys.* **1993**, *176*, 289−649 (Special Issue on Electron Transfer).
(6) For a list of many systems, see: Canters, G. W.; Dennison, C. *Biochimie* **1995**, *77*, 506−515.
(7) Bendall, D. S., Ed. *Protein Electron Transfer*; BIOS: Oxford, 1996.
(8) *J. Biol. Inorg. Chem.* **1998**, *3*, 195−225 and references therein. (Commentaries on electron-transfer mediated by DNA).
(9) Jortner, J.; Bixon, M., Eds. *Electron Transfer from Isolated Molecules to Biomolecules*; Advances in Chemical Physics 106 and 107, Parts I and II; J. Wiley: New York, 1998.
(10) Kuznetsov, A. M.; Vigdorovich, M. D.; Ulstrup, J. *Chem. Phys.* **1993**, *176*, 539−554.
(11) Kuznetsov, A. M.; Ulstrup, J. *Spectrochim. Acta A* **1998**, *54A*, 1201−1209.
(12) Mahler, G.; May, V.; Schreiber, M., Eds. *Molecular Electronics*; M. Dekker: New York, 1996.
(13) *Molecular Electronics*; Jortner, J.; Ratner, M., Eds.; Blackwell: Oxford, 1997.
(14) Chen, C. J. *Introduction to Scanning Tunneling Microscopy*; Oxford University Press: New York, 1993.
(15) Magonov, S. M.; Whangbo, M.-H. *Surface Analysis with STM and AFM*; Verlag Chemie: Weinheim, 1996.
(16) Lipkowski, J., Ross, P. N., Eds. *Imaging of Surfaces and Interfaces*; Wiley-VCH: New York, 1999.
(17) Lindsay, S. M.; Li, Y.; Pan, T.; Thundat, T.; Nagahara, L. A.; Oden, P.; DeRose, J. A.; Knipping, U.; White, J. W. *J. Vac. Sci. Technol. B* **1991**, *9*, 1096−1101.
(18) Lee, I.; Lee, J. W.; Warmack, R. J.; Allison, D. A.; Greenbaum, E. *Proc. Natl. Acad. Sci. U.S.A.* **1995**, *92*, 1965−1969.
(19) Samanat, M. P.; Tian, W.; Datta, S.; Henderson, J. I.; Kubiak, C. P. *Phys. Rev. B* **1996**, *53*, R7626−R7629.
(20) Datta, S.; Tian, W.; Hong, S.; Reifenberger, R.; Henderson, J. I.; Kubiak, C. P. *Phys. Rev. Lett.* **1997**, *70*, 2530−2533.
(21) Dhirani, A.; Lin, P.-H.; Guyot-Sionnest, P.; Zehner, R. W.; Zita, L. R. *J. Chem. Phys.* **1997**, *106*, 5249−5253.
(22) Sautet, P. *Chem. Rev.* **1997**, *97*, 1097−1116.
(23) Claypool, C. L.; Fagloini, F.; Goddard, W. A., II; Gray, H. B.; Lewis, N. LS.; Marcus, R. A. *J. Phys. Chem. B* **1997**, *101*, 5978−5995.
(24) Lu, X.; Hipps, K. W. *J. Phys. Chem.* **1997**, *101*, 5391−5396.
(25) Danilov, A. I. *Russ. Chem. Rev.* **1995**, *64*, 767−781.
(26) Gewirth, A. A., Siegenthaler, H., Eds. *Nanoscale Probes of the Solid/Liquid Interface*; Kluwer: Dordrecht, 1995.
(27) Gewirth, A. A.; Niece, B. K. *Chem. Rev.* **1997**, *97*, 1129−1162.
(28) Höltze, M. H.; Wandlowski, T.; Kolb, D. M. *J. Electroanal. Chem.* **1995**, *394*, 271−275.
(29) Wandlowski, T.; Lampner, D.; Lindsay, S. M. *J. Electroanal. Chem.* **1996**, *404*, 215−226.
(30) Nyffenegger, R. M.; Penner, R. M. *Chem. Rev.* **1997**, *97*, 1195−1230.
(31) Andersen, J. E. T.; Ulstrup, J.; Møller, P. *Electrochemical Nanotechnology*; Lorenz, W. J., Plieth, W., Eds.; Wiley-VCH: Weinheim, 1998; pp 27−44.
(32) Kolb, D. M.; Ullmann, R.; Will, T. *Science* **1997**, *275*, 1097−1099.
(33) (a) Kuznetsov, A. M.; Ulstrup, J. *Chem. Phys.* **1991**, *157*, 25−33. (b) Kuznetsov, A. M.; Sommer-Larsen, P. Ulstrup, J. *Surf. Sci.* **1992**, *275*, 52−64. (c) Kuznetsov, A. M.; Ulstrup, J. *Surf. Coat. Technol.* **1994**, *67*, 193−200.
(34) Friis, E. P.; Kharkats, Yu. I.; Kuznetsov, A. M.; Ulstrup, J. *J. Phys. Chem. A* **1998**, *102*, 7851−7859.
(35) Sumi, H. *J. Phys. Chem. B* **1998**, *102*, 1833−1844.
(36) Schmickler, W. *Surf. Sci.* **1993**, *295*, 43−56.
(37) Kuznetsov, A. M.; Ulstrup, J. *Elektrokhimiya* **1995**, *31*, 244−249.
(38) Dogonadze, R. R.; Kuznetsov, A. M.; Vorotyntsev, M. A. *Croat. Chim. Acta* **1972**, *44*, 257−273.
(39) Kuznetsov, A. M.; Ulstrup, J. *J. Electroanal. Chem.* **1985**, *195*, 1−19.
(40) Schmickler, W. *J. Electroanal. Chem.* **1986**, *204*, 31−43.
(41) Sebastian, K. L.*J. Chem. Phys.* **1989**, *90*, 5056−5067.
(42) Smith, B. B.; Hynes, J. T. *J. Chem. Phys.* **1993**, *99*, 6517−6530.
(43) Boroda, Yu. G.; Voth, G. A. *J. Electroanal. Chem.* **1998**, *450*, 95−107.
(44) Frauenfelder, H.; Wolynes, P. *Science* **1985**, *229*, 337−345.
(45) Kuznetsov, A. M.; Schmickler, W. Work in progress.
(46) Andersen, J. E. T.; Møller, P.; Pedersen, M. V. *Surf. Sci.* **1995**, *325*, 193−205.
(47) Zhang, j.; Chi, Q.; Dong, S.; Wang, E. *Bioelectrochem. Bioeng.* **1996**, *39*, 267−274.
(48) Friis, E. P.; Andersen, J. E. T.; Madsen, L. L.; Møller, P.; Ulstrup, J. *J. Electroanal. Chem.* **1997**, *431*, 35−38.
(49) Friis, E. P.; Andersen, J. E. T.; Kharkats, Yu. I.; Kuznetsov, A. M.; Nichols, R. J.; Zhang, J.-D.; Ulstrup, J. *Proc. Natl. Acad. Sci. U.S.A.* **1999**, *96*, 1379−1384.
(50) Chi, Q.; Zhang, J.; Nielsen, J. U.; Friis, E. P.; Chorkendorff, I.; Canters, G. W.; Andersen, J. J. E. T.; Ulstrup, J. *J. Am. Chem. Soc.* **2000**, *122*, 4047−4055.
(51) Snyder, S. R.; White, H. S. *J. Electroanal. Chem.* **1995**, *394*, 177−185.
(52) Han, W.; Durantini, E. N.; Moore, T. A.; Moore, A. L.; Gust, D.; Rex, P.; Leatherman, G.; Deely, G. R.; Tao, N.; Lindsay, S. M. *J. Phys. Chem. B* **1997**, *101*, 10719−10725.
(53) Tao, N. J. *Phys. Rev. Lett.* **1996**, *76*, 4066−4069.
(54) Schmickler, W.; Tao, N. J. *Electrochim. Acta* **1997**, *42*, 2809−2815.